Conductive hydrophobic graphene oxide films via laser-scribed surface modification

Apsey, Henry; Hill, Donald; McCoy, Thomas M.; Villeda-Hernandez, Marcos; Faul, Charl F.J.; Alexander, Shirin

DOI
10.1016/j.jcis.2025.02.055

Publication date
2025

Document Version
Final published version

Published in
Journal of Colloid and Interface Science

Journal of Colloid and Interface Science 687 (2025) 189–196

Contents lists available at ScienceDirect

Journal of Colloid And Interface Science

journal homepage: www.elsevier.com/locate/jcis

Regular Article

Conductive hydrophobic graphene oxide films via laser-scribed surface modification

Henry Apsey [a,1], Donald Hill [a,2], Thomas M. McCoy [b], Marcos Villeda-Hernandez [c], Charl F.J. Faul [c,3], Shirin Alexander [a,*,4]

[a] Department of Chemical Engineering, Swansea University Bay Campus, Fabian Way, Swansea SA1 8EN UK
[b] Department of Radiation Science and Technology, Technische Universiteit Delft, Delft 2629JB The Netherlands
[c] School of Chemistry, University of Bristol, Bristol BS8 1TS UK

GRAPHICAL ABSTRACT

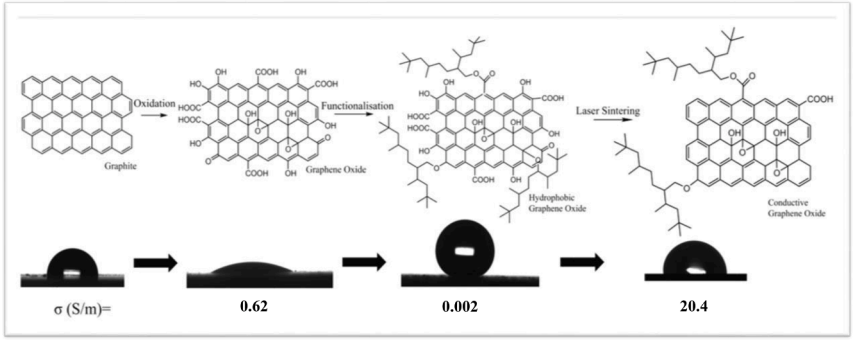

ARTICLE INFO

Keywords:
Wettability
Wearable electronics
Conductive
Waterproof
Water-repellent
Carbon materials
Biosensors

ABSTRACT

Graphene oxide (GO) can be surface modified for various purposes, including enhancing its properties or tailoring its behaviour for specific applications such as biosensing. Herein we report the behaviour of a carboxylate functionalized graphene oxide that is both water repellent and electrically conductive. The GO is first produced using a modified Hummers method and then functionalized with a hyperbranched isostearic alcohol through an esterification reaction. The as-deposited functionalized GO films were observed to cause "petal-like" wetting of water, whereby droplets exhibited contact angles (CAs) greater than 150° and remaining pinned to the surface. To improve their conductivity, films of the functionalized GO deposited onto glass were laser-scribed to reduce some of the specific, adjoining regions of oxidic carbon to partially restore some of the sp^2 C network. This improved the conductivity of the as-deposited GO films by approximately four orders of magnitude from 0.002 to ~20 S/m using the low laser scan speed of 250 mm/min. It was observed that with a high laser scan speed of 500 mm/min some of the hydrophobic character was retained (CAs ~110°), whilst maintaining conductivities of up

* Corresponding author.
E-mail address: s.alexander@swansea.ac.uk (S. Alexander).
[1] ORCID: https://orcid.org/0000-0001-6095-7646.
[2] ORCID: https://orcid.org/0000-0002-3457-5895.
[3] ORCID: https://orcid.org/0000-0001-6224-3073.
[4] ORCID: https://orcid.org/0000-0002-4404-0026.

https://doi.org/10.1016/j.jcis.2025.02.055
Received 8 November 2024; Received in revised form 20 January 2025; Accepted 8 February 2025
Available online 10 February 2025

to 0.17 S/m. Consequently, these materials show promise for applications such as biosensing materials, where tuneable hydrophobicity combined with conductivity are required characteristics.

1. Introduction

Carbon-based materials, including carbon nanotubes (CNTs), graphene, and carbon black, are commonly used for various applications including water-repellent coatings, water filtration, electronics, energy storage and bioelectric sensors due to their high electrical conductivity, large surface area, and biocompatibility [1,2]. These materials are often incorporated into electrode structures to enhance signal detection sensitivity and improve electrochemical performance in various sensing applications; however, they can be susceptible to damage from water or other liquids [2–4].

Carbon-based materials have long been used to make hydrophobic coatings due to their low surface energy, high surface area and structural stability [5,6]. Materials such as graphene, carbon nanotubes, carbon nanofibers, and carbon black, can undergo surface modifications to achieve hydrophobicity [7–9]. Functionalization alters their surface chemistry, enhancing their utility in various applications [2,9–13]. Surface modification involves chemical treatments that introduce hydrophobic groups to the surface. This can include alkyl chains or fluorinated groups, which can change the affinity of the surface for water, making it repel water droplets (i.e. hydrophobic) [14].

Among other carbon-based materials, graphene, a two-dimensional material consisting of a single layer of carbon atoms arranged in a hexagonal lattice, exhibits extraordinary electrical conductivity ($> 10^4$ S/m), owing to the high mobility of electrons within its structure sp^2 delocalised carbon framework. This allows the electrons in graphene to move ballistically over long distances without scattering, making it one of the most electrically conductive materials known. Although graphene offers inherently high conductivity due to its sp^2 hybridized network, it lacks the functional groups needed for further reactions, which limits its chemical tunability. In contrast, graphene oxide (GO), a derivative of graphene, consists of oxygen-containing functional groups such as hydroxyl, epoxy, and carboxylic groups covalently attached to its carbon framework. This makes GO a versatile platform where properties like wettability and conductivity can be tailored through functionalization and reduction. These groups attach onto sp^3 carbons that form in the structure because of a well-studied oxidation process, the Hummers method, using sulfuric acid (H_2SO_4) and potassium permanganate ($KMnO_4$) [15]. This results in a disrupted hexagonal lattice that is no longer homogeneous as with graphene. Most carbon atoms maintain sp^2 hybridization but the increased number of sp^3 hybridized carbon atoms significantly reduces the electronic delocalisation, thus lowering the conductivity (< 1 S/m).

The presence of oxygen-containing functional groups, such as alcohols, ethers and carboxylic acid groups, introduced by the oxidation alters its surface energy, making it more hydrophilic and thus more dispersible in water and other polar solvents. This behaviour renders GO more compatible with aqueous processing routes, thus extending the utility of the material use in aqueous environments [12,16]. In addition, the presence of these functional groups also provides avenues to further functionalization through their reactivity. Functionalization of GO can also be achieved using alcohols and alkyl alkoxysilanes, which further allows tailoring of the materials' chemistry and surface energy through reaction with the pendant oxidic groups through condensation reactions [4,8,12,17].

It has also been shown that thermal and/or photothermal reduction can be performed to partially restore the sp^2 C network, to form what has been termed reduced graphene oxide (rGO). Laser-scribing can partially restore sp^2 C, increasing the material's conductivity by several orders of magnitude. Laser-scribing is an attractive method for reducing GO given its ability to locally control the reduction process, by allowing the laser to selectively interact with discrete areas of the film. Briefly, a laser source, typically in the near-infrared range, is directed onto the surface of the GO film. The laser's energy is then absorbed by the material, resulting in localized heating and inducing thermal decomposition of oxygen-containing functional groups (hydroxyl, epoxy, carboxyl etc). The removal of oxygen-containing functional groups results in the restoration of the planar sp^2 structure and thus an increase in conductivity. Laser-scribed graphene oxide has been used in the development of conductive films, electrodes, and supercapacitors, and materials used in other electronic and energy-related applications [18,19]. Another application of GO and rGO is in the field of biosensors, as result of their inherent biocompatibility [20,21]. This biocompatibility is intimately linked to the wettability of the material since the adsorption of biomolecules onto surfaces is assisted by the presence of hydrophilic groups.

Although the oxidic functionalities of GO are desirable for use in aqueous environments, there is a drive to investigate whether the reactive functional groups can be further exploited to manufacture water-proof conductive coatings that can be used outdoors where they are susceptible to degradation from weathering. Tuning the wettability of the material from hydrophilic to hydrophobic is achieved by reacting the GO with non-fluorinated, hyperbranched alcohol, resulting in a non-hazardous environmentally friendly compound (Scheme 1). The approaches taken in this research enable tunable properties, such as selectively restoring sp2 domains for targeted conductivity while retaining functionalized hydrophobicity. Although more complex, this approach balances performance and practicality, making it suitable for applications like biosensors, where biocompatibility and controlled surface properties are critical. Moreover, hydrophobic graphene oxide's large surface area and chemical tunability enhance its interaction with specific biomolecules, making it ideal for detecting various analytes in real time. In this paper, we demonstrate that it is possible to create highly hydrophobic graphene oxide films that display petal-like wetting from water droplets (CAs >150°). Furthermore, we also show that this material can be laser-scribed to improve its conductivity by several orders of magnitude compared to untreated GO while retaining its hydrophobic properties (CAs ~110°) (Scheme 1).

2. Materials and methods

2.1. Materials

Graphite flakes, sulfuric acid, phosphoric acid, hydrogen peroxide and potassium permanganate were purchased from Merck Life Sciences. Fineoxocol180 alcohol (2,2,4,8,10,10-hexamethylundecan-5-ol) (FO180) was provided by Nissan Chemical Industries. Ethanol (99.5 %), and isopropanol (99.5 %) were purchased from Merck Life Sciences. Glass slides were acquired from Avantor (VWR).

2.2. Graphene oxide synthesis

Modified graphene oxide (GO) was synthesized by a modified Hummers' method [22]. In this variation, a concentrated mixture of H_2SO_4/H_3PO_4 (360:40 mL, 9:1 ratio) was combined with graphite flakes (3.0 g, 1 wt equiv) and $KMnO_4$ (18.0 g, 6 wt equiv). The reaction was then heated to 50 °C and stirred for 12 h. The reaction was then cooled to 25 °C and poured onto ice (~400 mL) with 30 % H_2O_2 (3 mL). The remaining material was shaken and sieved through a 300 μm filter to remove large particles. The filtrate was centrifuged (5000 rpm for 4 h), and the supernatant decanted away. This was centrifuged and washed in the same method described above. The residual material, after multiple

washes, was coagulated with 200 mL of ether, and the resulting suspension was filtered. The solid obtained from the filtration was vacuum-dried for 3 days at a temperature of 30 °C, yielding 2.4 g of the final product.

2.3. Functionalisation of graphene oxide with finoxocol (FO180) (2,2,4,8,10,10-hexamethylundecan-5-ol)

Under ventilated fume hood conditions, 100 mg GO was suspended in 10 mL of concentrated sulfuric acid and sonicated for 15 min. 90 ml of chloroform was added and this was stirred and gently heated to 80 °C over 1 h. FO180 (5 mL) was added dropwise to the mixture over an hour. The heating was stopped to allow the mixture to cool to room temperature and then stirred for 24 h. Preliminary tests were found that the time given was sufficient to ensure the reaction occurred with the desired wettability (WCA> 150°), this level of wettability falls within the threshold for superhydrophobic materials and was thus deemed comparable with literature. The unreacted alcohol was removed by washing with isopropanol and then centrifuging the mixture at 5000 rpm for one hour to recover the solid. The supernatant was then discarded, and the process was repeated using ethanol. The functionalized material was then dried at 100 °C for 24 h. The initial synthesis was repeated, resulting in materials with contact angles ranging from 144° to 151°. This small range of wettability after the first synthesis demonstrates the reproducibility of the process. Consequently, a large batch was synthesized to conduct all other characterizations, coatings, and electrical conductivity measurements. This approach ensured that all coatings and characterizations were performed on the same batch, allowing for cross-comparability.

2.4. Spray coating

Graphite, GO, fGO and rGO were dispersed in isopropanol to prepare 2 %wt. suspensions and then spray coated onto glass microscope slides using a compressed air propellant spray gun with a pressure of 20 psi. Multiple coats were applied to ensure the films fully covered the surface of the substrate. The films produced are robust enough to undergo characterizations without fracturing. However, they can be removed by percussive abrasion, cracking off as flakes when strong mechanical force is applied due to the lack of adhesion between the glass substrate and the particles.

2.5. Laser-scribing

Reduced Graphene Oxide (rGO) films on glass sides were obtained using a desktop laser engraver with 405 nm laser diode a and a power of 250 mW [23]. The focal length of the diode module was set to 40 mm. The spatial resolution of the engraver was 0.1 mm. GO films were laser-

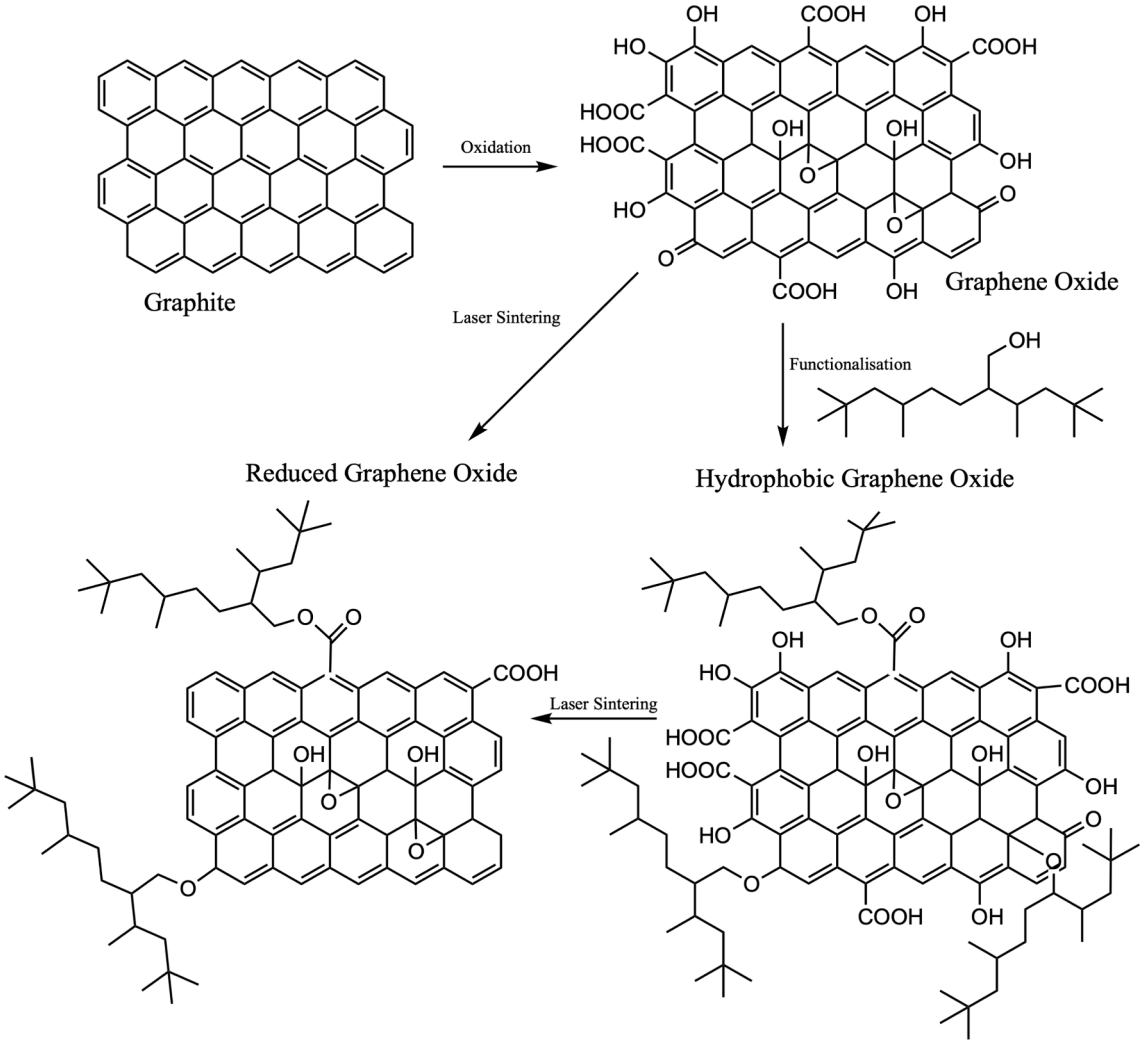

Scheme 1. Reaction scheme showing the various steps taken for graphite modification: the oxidation of graphite to graphene oxide, the reaction with FO180 to form hydrophobic graphene oxide and laser-scribing to form reduced graphene oxide.

scribed by continuous scanning in a raster pattern. Laser power was pulse-width modulation controlled and set to 60 % duty cycle. The film surface was placed 6 mm out of focus (46 mm distance from the lens) to increase line width and ensure interconnection between adjacent lines. Two laser scan speeds of 500 and 250 mm/min were used with a typical scan size of 20 x 20 mm. Film resistivity (ρ) was calculated using a standard 4-point probe where a voltage and current were applied between two outside probes, while the voltage was monitored through internal probes. [24–26] The measured resistance (R, Ω) was converted to sheet resistance (R_s, Ω/sq.) by the following relationship (Eq. (1)).

$$R_s = R \times f_1 f_2 \frac{\pi}{\ln(2)} \quad (1)$$

where f_1 and f_2 are the geometric correction factor that takes into consideration the specific sample dimensions to account for possible current path limits caused by the sample edges. f_1, accounts for the finite thickness of the sample and is equal to 1. f_2, accounts for the finite length and width of the sample, and it is equal to 0.82. The details on the calculation of f_2 are provided in the Supporting Information.

Conductivity (σ, S/m) values were calculated using Eq. (2), where ρ is the resistivity (Ω·m), and t is the sheet thickness in meters.

$$\sigma = \frac{1}{\rho} = \frac{1}{R_s \times t} \quad (2)$$

Approximate thickness (100 μm) was measured using optical microscopy at 500x magnification, with film samples placed on their side and then measured against the thickness of the glass slide (Fig. S1).

The laser scriber parameters—power, speed, and frequency—are software-controlled and can be precisely tuned to achieve various irradiation results. The greater the energy delivered per unit of surface area, the deeper the laser penetration. This approach allows control over the depth at which the irradiation penetrates the GO-based material, transforming the GO into conductive and hydrophobic laser-induced graphene. With the right tuning, the laser can easily penetrate GO-based surfaces to depths on the order of millimetres.

2.6. Characterization

X-ray photoelectron spectroscopy (XPS) was performed using an Axis Supra XPS fitted with a monochromated Al Ka source and large area slot mode detector (ca. 300 × 800 μm^2 analysis area). Spectra were recorded using a charge neutralizer to limit differential charging and binding energies were calibrated to the main hydrocarbon peak (BE 284.8 eV). XPS data was analyzed using CASA software with Shirley background. Scanning electron microscopy (SEM) and associated energy dispersive X-ray (EDX) were performed using a Hitachi Field Emission TM3030 scanning microscope in BSE mode with an accelerating voltage of 1.0 kV. Thermogravimetric Analysis (TGA) was performed using approximately 20 mg samples of powder into a TA Instruments SDT-Q600 analyzer, heating from ambient temperature to 600 °C under a 100 mL/min continuous flow of argon and a heating rate of 10 °C/min. Raman spectroscopy was performed using a Renishaw inVia Raman microscope with a laser wavelength of. Beam power of 5 % was used for data acquisition between 100 cm^{-1} and 3200 cm^{-1}. Fourier transform infrared spectroscopy (FTIR) was performed with an average of 16 scans, recording spectra between 400–4000 cm^{-1} region, using a Perkin Elmer Spectrum 2 with Universal Attenuated Total Reflectance (UATR) accessory. Contact angle measurements were performed using a Krüss DSA 25 with an IDS UI-306xCP-M camera using Advance software. A Young Laplace fitting method was used to calculate the contact angles. Distilled water (Millipore, 18 MΩ cm) was used during all measurements as the dispersed phase. Measurements were taken at three different locations across the surfaces using 5 μL droplets and a dosing rate of 2.66 μL s^{-1}. Where appropriate, pellets of material were prepared for testing using a hydraulic press (20 wt% added water, 200 mg sample, 5 mm die, 1 t, 30 s). Pellets were prepared for XPS, SEM and wettability measurements on the pellets themselves. Note that although various batches were synthesized to examine reproducibility, all the characterization data presented are from one large batch to ensure cross-comparability.

3. Results & discussion

3.1. Characterisation of the GO samples

GO was synthesised using modifications of the Hummers method to optimise the atomic percentages of oxygen and functional groups upon the carbon backbone. Analysis of the atomic percentages recorded from the XPS survey spectra of both graphite (SI Figs. S2) and GO (Fig. S3) showed substantially higher proportions of oxygen in GO (~ 30 %) relative to samples of the as-received graphite precursor (~ 4 %) as is shown in Table 1, suggesting the presence of oxidic carbon. The high-resolution XPS scans for the C 1s region of graphite, and GO are shown in Fig. S4. For graphite, only C—C bonds are present at 284.6 eV, while for GO samples the data were fitted to the C—C bonds at 284.6 eV corresponding to the sp^2 carbon along with additional C—O and O—C═O peaks at 285.4 and 286.48 eV respectively, due to epoxy and carboxylic functional groups [27].

EDX was also performed on microscope slides coated with graphite and GO samples to study whether the bulk composition reflected that of the surface. This was largely observed, as presented in Table 1 and Figs. S5 & S6 of Supporting information. The small silicon peak is likely to have originated from contamination during the preparation, handling, or characterising process. Other ions present in some samples are potassium, most likely left over from the oxidizing agent $KMnO_4$, chlorine from the chloroform and phosphorus ions are also potentially present intercalated between the layers of graphene oxide likely from the phosphoric acid which can be accommodated easily due to expanded interlayer distance in graphene oxide and its electrostatic potential [28]. Doping with some of these ions may be desirable for some applications [29–32].

Raman spectroscopy data (Fig. 1) show graphite has a larger G band (~1580 cm^{-1}) which corresponds to the in-plane vibrations of the sp^2-bonded carbon atoms (the E_2g phonon mode). The G-band is a signature of ordered graphitic structures, indicating the presence of crystalline graphite. The D-band (~1350 cm^{-1}) appears when there are defects or disorders in the graphite structure. The D-band is attributed to the breathing mode of the sp^2 rings but requires the presence of disorder (e.g., edges, impurities, or structural defects) to be activated (a process known as defect-activated Raman scattering). Graphene oxide data (Fig. 1b) exhibits an even ratio of D/G bands, a measure of the defects present in a graphene structure (the irregularities of the crystal lattice structure). These defects introduce localized disruptions in the carbon lattice and contribute to the overall disorder and heterogeneity of graphene oxide.

3.2. Functionalization of graphene oxide samples with hyperbranched alcohol FO180

GO was functionalized with a hyper-branched alcohol, FO180, to alter the wettability of the GO films, in the manner shown in Scheme 1 and characterised using IR spectroscopy, TGA, and contact angle (CA) measurements.

Table 1
Atomic percentages of graphite and GO samples determined by EDX and XPS.

Sample	C 1s	O 1s	S 2p
Graphite (EDX) %	100.00	0	0
Graphite (XPS) %	93.85	4.59	1.56
GO (EDX) %	64.00	34.65	0.48
GO (XPS) %	68.06	30.53	1.41

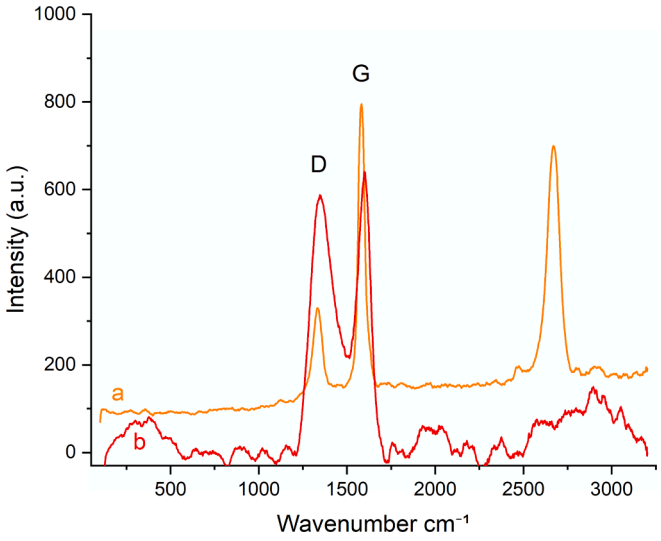

Fig. 1. Raman spectroscopy of a) graphite, and b) Modified graphene oxide.

The IR spectra of the graphite, graphene oxide and functionalised GO are shown in Fig. 2 (IR of the FO180 alcohol is shown in Fig. S11). As expected, there are not many peaks available in the graphite spectrum due to the absence of functional groups. However, GO showed distinct peaks that could be ascribed to O—H (alcohols, phenols), C═O, and C—O stretching at 3340, 1633–1717, and 1031–1159 cm^{-1} respectively. In this case, the position of the C═O band is more consistent with the presence of ketones as well as those reported for carboxylic acid groups attached to aromatic rings, indicating that CO_2H groups could be attached to sp^2 carbon atoms at the edges of the sheets. The two bands at around 1100–1200 cm^{-1}, are ascribed to C—O stretching of the alcohols as well as more tentatively epoxides since these have also been reported as functional groups on GO. [33] In addition, a weak band around 2982 cm^{-1} is also observed indicating some C—H stretching of sp^3 C in the structure. IR spectrum of fGO (Fig. 2c) shows strong multiple C—H stretching bands after exposure to FO180 at about 2917 cm^{-1}, as well as two peaks at around 1370 and 1450 cm^{-1} due to the C—H rock and bend respectively, indicating the presence of the alkyl chain of FO180 alcohol in the sample. [34] There is also a noticeable C═O stretch peak at 1702 cm^{-1} due to the presence of the esters (which are still present after purification and sonication) indicating chemical absorption of FO180 via esterification reaction. [35].

TGA was used to further characterize the composition and thermal stability of the samples as is shown in Fig. 3. It was observed through studying the derivative curves that the graphite precursor (Fig. 3a) started to thermally decompose at around 700 °C with complete thermal decomposition and the breaking of C—C bonds at approximately 900 °C. By comparison, GO (Fig. 3b), has lower thermal stability and began decomposing under the same conditions at a much lower temperature (~ 400–500 °C) with complete C—C decomposing at ~700 °C. This is consistent with what has previously been reported [36] for this type of oxygen-containing functional groups such as hydroxyl (—OH), epoxy (C—O—C), and carboxyl (—COOH) groups which require less energy to decompose. It is noteworthy that GO retains around 15 % residue after complete C—C decomposition at approximately 700 °C. This residue could be attributed to inorganic impurities introduced during the synthesis step, as well as contamination during the preparation, handling, or characterization processes. The samples functionalised with branched alcohol have ~20 % weight loss between 200–300 °C which is attributed to the branched hydrocarbon groups of FO180 with complete decomposition around 500 °C representing the final stages of GO, where the carbon framework itself starts to break down, leaving behind carbonaceous residue. These results indicate that the thermal stability of the samples is proportional to the strength of the sp^2 hybridized carbon atoms in a hexagonal carbon framework and increasing defectiveness, such as the presence of GO and sp^3 hybridized carbon via functionalisation will reduce it significantly.

To see the effect of functionalization on the wettability of the films, water contact angle (WCA) measurements were performed. Graphite films were borderline hydrophobic, showing a WCA of about 90° (Fig. 4a). By comparison, films prepared from GO were highly hydrophilic and showed a WCA of about 10° because of the O-containing polar groups introduced into the structure because of the oxidation (Fig. 4b). Upon further reaction of the GO particles with the hyperbranched low surface energy alcohol, the wettability of the films was altered significantly and the WCA increased to around 150° (Fig. 4c, Fig. S12). However, the GO film was observed to display petal-like wettability as water droplets were observed to remain pinned to the surface of the film, even after tilting to angles greater than 90°. The high water contact angle is as a direct consequence of increasing the CH_3:CH_2 ratio per chain because of branching, hence exposing more —CH_3 groups with the "hedgehog" tail structures which have a lower surface free energy

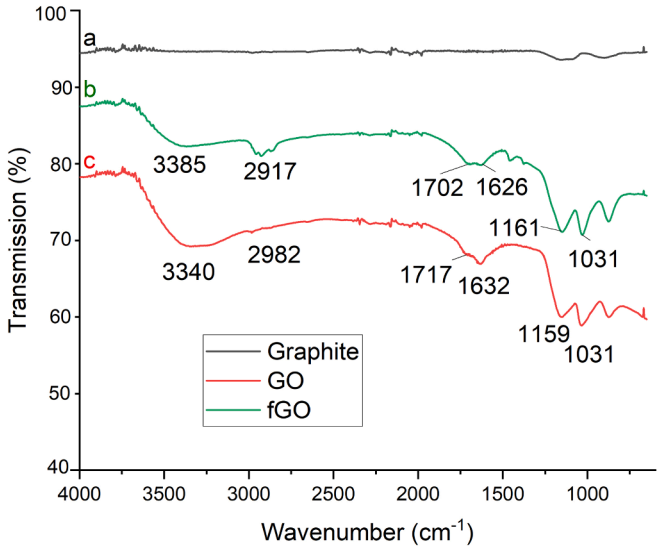

Fig. 2. FTIR spectra of (a) graphite, (b) modified graphene oxide (GO), (c) functionalised graphene oxide with F180 (fGO). Data have been shifted vertically to see the clarity of the peaks.

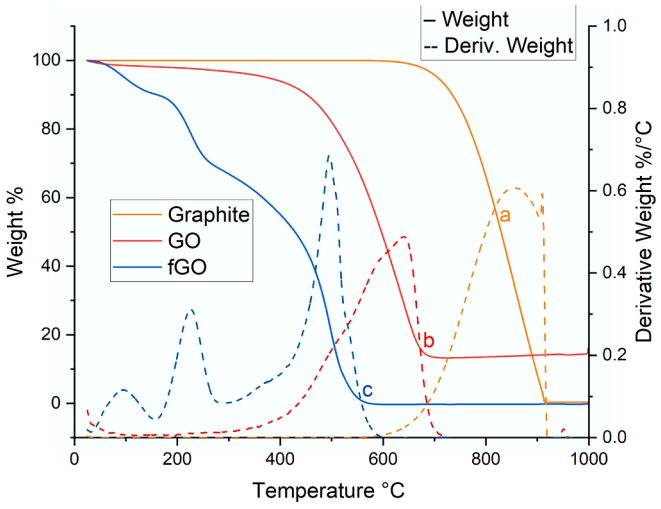

Fig. 3. TGA plot for a) Graphite, b) modified graphene oxide (GO), and c) functionalised graphene oxide (fGO), showing Weight % (- solid lines) and Derivative Weight (– dashed lines) against Temperature.

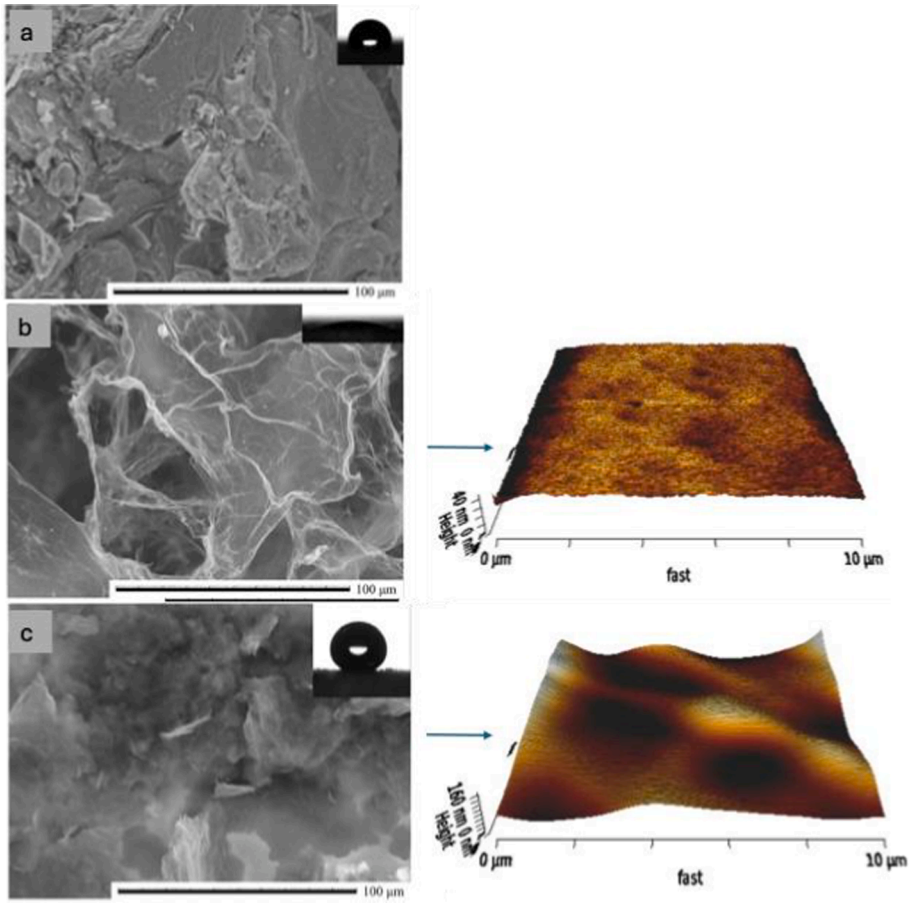

Fig. 4. SEM images (1000× magnification) of films spray-coated onto a microscope slide of a) graphite b) graphene oxide, and c) functionalised graphene oxide along with the AFM images. Insets are images of water droplets on the corresponding surfaces. Note the very low contact angle of the water droplet on graphene oxide (b).

compared to —CH_2 groups. This is in line with our previous work, showing that alumina nanoparticles functionalized with hyper-branched carboxylic acids possessed superhydrophobic properties in line with fluorocarbon analogue [37,38]. Functionalization was also confirmed by examining the dispersibility of the material in different solvents. Prior to the reaction with FO180, the GO samples could be well dispersed in water and polar solvents such as ethanol, whereas after functionalization the material could only be dispersed in non-polar solvents (See Fig. S13) like hexane, suggesting that there were far fewer hydrogen bonding interactions taking place between particles and water molecules.

Surface structure analysis of the graphite sample showed that the film possessed a rough morphology at the microscale (Fig. 4a, Figs. S7–8, Fig. S14). However, upon modification, both SEM and AFM revealed that the GO film was smooth at the nanoscale and showed very low surface roughness values (R_q ~10 nm) (Fig. 4b and S9–10). Upon functionalization of GO surfaces with low surface energy groups, the roughness increased to around R_q ~50 nm as is shown in Fig. 4c. Notably, this value is substantially lower than what we have observed previously for superhydrophobic Al_2O_3 nanoparticle films [38] that were functionalized by a carboxylic acid with the same hyperbranched chain (R_q ~110 nm), suggesting that the absence of superhydrophobic behavior is due to the lower nanoscale roughness of the functionalized GO films.

3.3. Conductivity measurements

Four-point probe measurements were used to record the resistivity of the different GO films. The values obtained were then converted into conductivity values using the reciprocal relationship stated in section 2.5. Both the GO and fGO films were observed to show conductivity several orders of magnitude lower than those reported for graphite films (as is shown in Table 2), which is ascribed to the oxidic sp^3 C in the GO samples reducing electron mobility. To examine whether the conductivity can be improved, laser-scribing at different speeds was used and it was observed to improve the conductivity substantially by thermally decomposing oxygen-containing functional groups (like hydroxyl, epoxy, and carboxyl groups) and partially restoring some of the sp^2 C network. As anticipated, the time that the films were exposed to laser irradiation influenced their decomposition, as shown by the values obtained for the different scanning speeds in Table 2. The lower scan speeds were observed to create films that showed conductivities four orders of magnitude greater than before irradiation for fGO samples, whereas scanning twice the speed increased the conductivity by two orders of magnitude. The change in conductivity is greater for FO180-functionalized GO films compared to GO films. Although this

Table 2
Conductivity values for Graphene oxide-based materials after laser irradiation at high and low laser scan speed.

Sample	Initial Conductivity (S/m)	Conductivity at 500 mm/min laser scan speed (S/m)	Conductivity at 250 mm/min laser scan speed (S/m)
Graphite	200.57 ± 16.70	220.63 ± 0	220.63 ± 0
GO	0.62 ± 0	3.98 ± 0.01	3.97 ± 0.01
fGO	0.002 ± 0	0.17 ± 0.01	20.45 ± 0.20

phenomenon is not fully understood, there are two possible explanations:

1. The hyper-branched FO180 groups likely contribute to spacing and reducing inter-layer van der Waals forces within the GO structure. This can facilitate layer separation and prevent restacking during reduction, promoting a higher degree of structural order and more effective electron delocalization, leading to better electrical pathways after scribing.
2. The difference in conductivity may also be due to the film quality. Functionalized GO films are easily deposited as they are well dispersed in isopropanol and non-polar solvents (as shown in Fig. S13), leading to a coherent film with very few visible cracks. In contrast, non-functionalized GO films, despite being hydrophilic, are difficult to disperse in both polar and non-polar solvents, making it far more challenging to deposit a coherent film. These films exhibit less coherent morphology with some breaks in the coating. Fractures in the coating are responsible for lower conductivity, as they create a more difficult pathway for electron conduction.“

The WCA values of the films after the different speeds of laser-scribing are shown in Table 3 and reflect the varying degrees of decomposition. The WCA of GO reduced significantly to super-hydrophilic after laser-scribing due to increasing the roughness of the already hydrophilic surface. Notably, the WCA of the fGO films was also reduced, however, it was observed that hydrophobic contact angles could be obtained after laser-scribing of fGO sample after subjecting it to the higher laser scan speed. AFM showed that the fGO films increased topography ($R_q \sim 220$ nm) after laser irradiation, providing support that the drop in CAs was due to the removal of the hyperbranched alkyl groups of the esterified FO180 chains rather than the surfaces being made smoother because of the laser. (The AFM image of the reduced fGO film is shown in Fig. S9c). These data suggest that fGO materials could retain some utility as a water-repellent bioelectronic sensor if it was employed in the application.

Some studies have reported hydrophobic graphene oxide (GO) composites using polymers. Huang et al. [8] created graphene/graphene oxide nanocomposites and achieved maximum conductivity values of 2.7 S/m and a WCA of 120-135° using functionalisation with polymers such as polyacrylonitrile, which, when integrated into GO, can help to improve the dispersion of graphene within the matrix and create a more homogenous composite. Mizerska et al. also recorded conductivity values of 2.7 S/m and WCA of >140° with an organosilicon matrix (diethoxydimethylsilane, (3-glycidoxypropyl) triethoxysilane, tetraethoxysilane and polymethylhydrosiloxane) for use on cotton fabrics. [39] In the case of Mizerska et al., the use of an organosilicon matrix composed of compounds like diethoxydimethylsilane and (3-glycidoxypropyl) triethoxysilane suggests a different structural approach. Organosilicon compounds are known for creating robust, hydrophobic layers due to their ability to form a cross-linked network [40]. This network can encapsulate the GO sheets, reducing the availability of oxygen-containing groups that typically lower the electrical conductivity in GO. The organosilicon matrix likely enhances the overall hydrophobicity and preserves the conductive pathways within the film, leading to the observed conductivity. Composite films have a less homogeneous distribution of the conductive GO. In the cases of Huang et al. and Mizerska et al., [8,39] the polymers used seem to facilitate better dispersion and alignment of the GO compared to our samples, which is critical for achieving higher conductivity. Each method has achieved a balance between hydrophobicity and conductivity by carefully selecting its matrix materials and functionalization methods. Our method, the use of branched alcohols, is a cheap, green option to functionalise a conductive and hydrophobic carbon-based material.

Table 3
Water contact angles for Graphene-based materials before and after laser irradiation with improved conductivity.

Sample	Initial Contact Angle /°	WCA after 500 mm/min laser scan speed /°	WCA after 250 mm/min laser scan speed /°
Graphite	90.3 ± 3	91.6 ± 4	<1
GO	9.9 ± 5	<1	<1
fGO	150.5 ± 7	110.2 ± 8	95.4 ± 2

4. Conclusion

This study advances the current knowledge by presenting a comprehensive analysis of the synthesis of highly hydrophobic graphene oxide (GO) through chemical functionalization with highly branched alcohols. The subsequent laser-scribing reduction of this functionalized GO, once deposited on a surface, yields conductive hydrophobic materials. Our analysis demonstrates the production of an enhanced graphene oxide material [22], which shows significant potential for applications in coatings and biosensing.

Characterization methods such as IR, Raman Spectroscopy, XPS, and TGA confirmed the successful synthesis of graphene oxide using a modified Hummers method. This GO was then functionalized with a green hyper-branched low-surface energy alcohol (FO180) to adjust its wettability. Contact angle measurements revealed a significant reduction in water contact angle (from hydrophobic to highly hydrophilic) upon the addition of oxygen groups to the surface (graphite to GO reaction), whereas highly hydrophobic surfaces (WCAs > 150 °) were observed after functionalizing GO with FO180.

Conductivity tests at various modification stages, both before and after laser-scribing, showed that laser-reduced samples were significantly more conductive than the original graphene oxide, with an increase of 1000x in the case of functionalized GO (fGO). This enhanced conductivity is likely due to the removal of oxygen-containing groups and the restoration of the graphene lattice during the laser reduction process, along with the presence of remaining FO180 functional groups.

The combined properties of water repellency and electrical conductivity make laser-reduced functionalized graphene oxide highly desirable for applications in electronics, sensors, and energy storage devices. However, it may not be suitable for applications requiring high thermal stability (up to 700–800 °C).

Author contributions

The manuscript was written through the contributions of all authors. All authors have approved the final version of the manuscript.

CRediT authorship contribution statement

Henry Apsey: Writing – original draft, Visualization, Methodology, Formal analysis, Data curation, Conceptualization. **Donald Hill:** Writing – review & editing, Supervision, Methodology, Formal analysis. **Thomas M. McCoy:** Writing – review & editing, Methodology. **Marcos Villeda-Hernandez:** Writing – review & editing, Methodology, Formal analysis. **Charl F.J. Faul:** Writing – review & editing, Resources. **Shirin Alexander:** Writing – review & editing, Validation, Supervision, Methodology, Funding acquisition, Conceptualization.

Declaration of competing interest

The authors declare the following financial interests/personal relationships which may be considered as potential competing interests: Henry Apsey reports financial support was provided by Salts Healthcare Limited. If there are other authors, they declare that they have no known competing financial interests or personal relationships that could have

appeared to influence the work reported in this paper.

Acknowledgements

Financial support was provided by EPSRC DTP EP/R51312X/1 and Salts Healthcare. We would also like to acknowledge Andreas Meletiou for initial functionalization studies. Elvin Aliyev for his support in modifying our method for consistent graphene oxide synthesis. The authors would like to also thank Dr Chris Romero for helpful discussions.

Appendix A. Supplementary data

Additional Photographs, SEM, EDX, XPS and water droplets on fGO have been provided. Supplementary data to this article can be found online at https://doi.org/10.1016/j.jcis.2025.02.055.

Data availability

No data was used for the research described in the article.

References

[1] P. Zhang, B. Zhu, P. Du, J. Travas-Sejdic, Electrochemical and electrical biosensors for wearable and implantable electronics based on conducting polymers and carbon-based materials, *Chem. Rev.* 124 (2024) 722–767.
[2] A. O. Egbedina, O. P. Bolade, U. Ewuzie and E. C. Lima, Emerging trends in the application of carbon-based materials: A review, *J Environ Chem Eng*, DOI:10.1016/j.jece.2022.107260.
[3] A. Pal, V.G. Nadiger, D. Goswami, R.V. Martinez, Conformal, waterproof electronic decals for wireless monitoring of sweat and vaginal pH at the point-of-care, *Biosens. Bioelectron.* 160 (2020) 112206.
[4] C. Tang, K. Zhou, R. Wang, M. Li, W. Liu, C. Li, X. Chen, Q. Lu, Y. Chang, Wearable biosensors for human sweat glucose detection based on carbon black nanoparticles, *Anal. Bioanal. Chem.* 416 (2024) 1407–1415.
[5] A. Baldelli, A. Amirfazli, J. Ou, W. Li, Spray-on nanocomposite coatings: Wettability and conductivity, *Langmuir* 36 (2020) 11393–11410.
[6] Q. Zeng, H. Zhou, J. Huang, Z. Guo, Review on the recent development of durable superhydrophobic materials for practical applications, *Nanoscale* 13 (2021) 11734–11764.
[7] M. Megaraj, M. Keppannan, Fabrication of a superhydrophobic nanofibres by electrospinning, *Dig. J. Nanomater. Biostruct.* 12 (2017) 11–17.
[8] H.-D. Huang, Z. Guo, P. Yang, P. Chen, J. Wu, Electrical conductivity and hydrophobicity of graphene oxide-modified carbon nanofibers, *Chem. Phys. Lett.* 771 (2021) 138551.
[9] G. Hummer, J.C. Rasaiah, J.P. Noworyta, Water conduction through the hydrophobic channel of a carbon nanotube, Nature 414 (2001) 188–190.
[10] J. Liu, J. Tang, J.J. Gooding, Strategies for chemical modification of graphene and applications of chemically modified graphene, *J. Mater. Chem.* 22 (2012) 12435–12452.
[11] S.M. Mousavi, F.W. Low, S.A. Hashemi, N.A. Samsudin, M. Shakeri, Y. Yusoff, M. Rahsepar, C.W. Lai, A. Babapoor, S. Soroshnia, S.M. Goh, S.K. Tiong, N. Amin, *RSC Adv.* 10 (2020) 12851–12863.
[12] G. Wang, B. Wang, J. Park, J. Yang, X. Shen, J. Yao, Synthesis of enhanced hydrophilic and hydrophobic graphene oxide nanosheets by a solvothermal method, *Carbon N. Y.* 47 (2009) 68–72.
[13] M. Moradi, M. Rezaei, Construction of highly anti-corrosion and super-hydrophobic polypropylene/graphene oxide nanocomposite coatings on carbon steel: experimental, electrochemical and molecular dynamics studies, *Constr. Build. Mater.* 317 (2022) 126136.
[14] I.S. Bayer, Superhydrophobic coatings from ecofriendly materials and processes: a review, *Adv. Mater. Interfaces* 7 (2020) 2000095.
[15] W.S. Hummers, R.E. Offeman, *Preparation of Graphitic Oxide* (1958).
[16] J.S. Lee, J.C. Yoon, J.H. Jang, A route towards superhydrophobic graphene surfaces: surface-treated reduced graphene oxide spheres, *J. Mater. Chem. A Mater.* 1 (2013) 7312–7315.
[17] S.C. Vanithakumari, G. Jena, S. Sofia, C. Thinaharan, R.P. George, J. Philip, Fabrication of superhydrophobic titanium surfaces with superior antibacterial properties using graphene oxide and silanized silica nanoparticles, *Surf. Coat. Technol.* 400 (2020) 126074.
[18] Y. Zhao, Q. Han, Z. Cheng, L. Jiang, L. Qu, Integrated graphene systems by laser irradiation for advanced devices, *Nano Today* 12 (2017) 14–30.
[19] R. Kumar, A. Pérez del Pino, S. Sahoo, R.K. Singh, W.K. Tan, K.K. Kar, A. Matsuda, E. Joanni, Laser processing of graphene and related materials for energy storage: state of the art and future prospects, *Prog. Energy Combust. Sci.* 91 (2022) 100981.
[20] J. Peña-Bahamonde, H.N. Nguyen, S.K. Fanourakis, D.F. Rodrigues, Recent advances in graphene-based biosensor technology with applications in life sciences, *J. Nanobiotechnol.* 16 (2018) 75.
[21] H. Zhang, R. He, Y. Niu, F. Han, J. Li, X. Zhang, F. Xu, Graphene-enabled wearable sensors for healthcare monitoring, *Biosens. Bioelectron.* 197 (2022) 113777.
[22] D.C. Marcano, D.V. Kosynkin, J.M. Berlin, A. Sinitskii, Z. Sun, A. Slesarev, L. B. Alemany, W. Lu, J.M. Tour, Improved synthesis of graphene oxide, *ACS Nano* 4 (2010) 4806–4814.
[23] D.T. Kuhnel, J.M. Rossiter, C.F.J. Faul, Laser-scribed graphene oxide electrodes for soft electroactive devices, *Adv. Mater. Technol.* 4 (2019) 1800232.
[24] H. Okino, I. Matsuda, R. Hobara, Y. Hosomura, S. Hasegawa, P.A. Bennett, In situ resistance measurements of epitaxial cobalt silicide nanowires on Si(110), *Appl. Phys. Lett.* 86 (2005) 1–3.
[25] A. Venugopal, L. Colombo, E.M. Vogel, Contact resistance in few and multilayer graphene devices, *Appl. Phys. Lett.* 96 (2010) 013512.
[26] D.K. Schroder, in *Semiconductor Material and Device Characterization*, Wiley, 2005.
[27] S. Park, J. An, I. Jung, R.D. Piner, S.J. An, X. Li, A. Velamakanni, R.S. Ruoff, Colloidal suspensions of highly reduced graphene oxide in a wide variety of organic solvents, *Nano Lett.* 9 (2009) 1593–1597.
[28] Y. Chen, L. Qin, Y. Lei, X. Li, J. Dong, D. Zhai, B. Li, F. Kang, Correlation between microstructure and potassium storage behavior in reduced graphene oxide materials, *ACS Appl. Mater. Interfaces* 11 (2019) 45578–45585.
[29] S. Some, I. Shackery, S.J. Kim, S.C. Jun, Phosphorus-doped graphene oxide layer as a highly efficient flame retardant, *Chem. Eur. J.* 21 (2015) 15480–15485.
[30] X. Fan, H. Xu, S. Zuo, Z. Liang, S. Yang, Y. Chen, Preparation and supercapacitive properties of phosphorus-doped reduced graphene oxide hydrogel, *Electrochim. Acta* 330 (2020) 135207.
[31] A. Mansuroglu, M. Gencten, M.B. Arvas, M. Sahin, Y. Sahin, Investigation the effects of chlorine doped graphene oxide as an electrolyte additive for gel type valve regulated lead acid batteries, *J. Energy Storage* 64 (2023) 107224.
[32] D. Bouša, J. Luxa, V. Mazánek, O. Jankovský, D. Sedmidubský, K. Klímová, M. Pumera, Z. Sofer, Toward graphene chloride: chlorination of graphene and graphene oxide, *RSC Adv.* 6 (2016) 66884–66892.
[33] C. Nethravathi, M. Rajamathi, Chemically modified graphene sheets produced by the solvothermal reduction of colloidal dispersions of graphite oxide, *Carbon N. Y.* 46 (2008) 1994–1998.
[34] S. Kiani, D.R. Jones, S. Alexander, A.R. Barron, New insights into the interactions between asphaltene and a low surface energy anionic surfactant under low and high brine salinity, *J. Colloid Interface Sci.* 571 (2020) 307–317.
[35] E.C. Qin, M.E. Kandel, E. Liamas, T.B. Shah, C. Kim, C.D. Kaufman, Z.J. Zhang, G. Popescu, M.U. Gillette, D.E. Leckband, H. Kong, Graphene oxide substrates with N-cadherin stimulates neuronal growth and intracellular transport, *Acta Biomater.* 90 (2019) 412–423.
[36] F. Farivar, P. Lay Yap, R.U. Karunagaran, D. Losic, Thermogravimetric analysis (TGA) of graphene materials: effect of particle size of graphene, graphene oxide and graphite on thermal parameters, *C (Basel)*, 2021, 7, 41.
[37] S. Alexander, J. Eastoe, A.M. Lord, F. Guittard, A.R. Barron, Branched hydrocarbon low surface energy materials for superhydrophobic nanoparticle derived surfaces, *ACS Appl. Mater. Interfaces* 8 (2016) 660–666.
[38] D. Hill, H. Apsey, A.R. Barron, S. Alexander, Hybrid hydrocarbon/fluorocarbon nanoparticle coatings for environmentally friendly omniphobic surfaces, *ACS Appl. Nano Mater.* 4 (2021) 13664–13673.
[39] U. Mizerska, W. Fortuniak, T. Makowski, M. Svyntkivska, E. Piorkowska, D. Kowalczyk, S. Brzezinski, Electrically conductive and hydrophobic rGO-containing organosilicon coating of cotton fabric, *Prog. Org. Coat.* 137 (2019) 105312.
[40] H. Apsey, D. Hill, A.R. Barron, S. Alexander, Slippery alkoxysilane coatings for antifouling applications, *ACS Appl. Mater. Interfaces* 15 (2023) 17353–17363.